

# Gap maps and intrinsic diffraction losses in one-dimensional photonic crystal slabs

Dario Gerace and Lucio Claudio Andreani

*Istituto Nazionale per la Fisica della Materia and Dipartimento di Fisica “Alessandro Volta,”  
Università di Pavia, Via Bassi 6, I-27100 Pavia, Italy*

(Dated: October 24, 2018)

A theoretical study of photonic bands for one-dimensional (1D) lattices embedded in planar waveguides with strong refractive index contrast is presented. The approach relies on expanding the electromagnetic field on the basis of guided modes of an effective waveguide, and on treating the coupling to radiative modes by perturbation theory. Photonic mode dispersion, gap maps, and intrinsic diffraction losses of quasi-guided modes are calculated for the case of self-standing membranes as well as for Silicon-on-Insulator structures. Photonic band gaps in a waveguide are found to depend strongly on the core thickness and on polarization, so that the gaps for transverse electric and transverse magnetic modes most often do not overlap. Radiative losses of quasi-guided modes above the light line depend in a nontrivial way on structure parameters, mode index and wavevector. The results of this study may be useful for the design of integrated 1D photonic structures with low radiative losses.

PACS numbers: 42.25.Fx, 42.70.Qs, 42.79.Dj, 42.82.Et

## I. INTRODUCTION

Photonic crystals embedded in planar dielectric waveguides, also known as photonic crystal slabs, are intensively investigated as a promising route for the tailoring of photonic states.<sup>1–40</sup> Indeed, propagation of light can be controlled in these systems by the dielectric discontinuity of the slab waveguide in the vertical ( $z$ ) direction and by the photonic pattern in the  $xy$  plane. The geometry of a patterned waveguide gives considerable freedom in designing photonic structures (periodic or containing defects) that can be realized at near-infrared or optical wavelength by lithography and etching.

Most experimental investigations of photonic crystal slabs with a two-dimensional (2D) or one-dimensional (1D) periodic lattice concern in-plane transmission<sup>2,4,6,16</sup> or surface reflectance/transmittance measurements<sup>5,8,14,20,30,34,35</sup> with the purpose of determining the photonic gaps and the band dispersion. Structures containing defect states like linear waveguides in 2D lattices<sup>26</sup> or microcavities in 1D systems<sup>32,33,40</sup> are also being investigated. On the theoretical side, the study of photonic crystal slabs has been undertaken with plane-wave expansion,<sup>3,7,11,28,31</sup> scattering-matrix methods,<sup>9,25,29</sup> finite-difference time-domain (FDTD) calculations,<sup>15,22,27,28</sup> modal methods,<sup>12,17,18,19</sup> and perturbative approaches.<sup>10,23,39</sup> Recently, a finite-basis expansion method has been introduced.<sup>36–38</sup> Most of these papers concern 2D structures, either periodic or with linear defects. The theoretical study of 1D structures is restricted to a few papers and mostly focused onto the optical response in both in-plane<sup>17,19</sup> and out-of-plane<sup>29,34,35,39,40</sup> configurations.

Electromagnetic eigenmodes in photonic crystal (PC) slabs with a periodic pattern have notable differences as compared to the ideal reference systems (i.e., not waveguide-embedded), which are well known from the literature for the cases of both 1D<sup>41,42</sup> and 2D<sup>42</sup> period-

icities. A most important issue is the *light-line problem*: only photonic modes which lie below the light line of the cladding material (or materials, if the waveguide is asymmetric) are truly guided and stationary, while those lying above the light line in the first Brillouin zone are coupled to leaky waveguide modes and are subject to intrinsic radiative losses. These *quasi-guided modes* are actually resonances in a region of continuous energy spectrum, and for this reason they are more difficult to calculate than truly guided modes below the light line. Indeed, while the dispersion of guided modes can be obtained by a plane-wave expansion with a supercell in the vertical direction<sup>7</sup>, the frequencies and especially the losses of quasi-guided modes are most commonly studied by FDTD calculations.<sup>24</sup> Another important feature of photonic crystal slabs is the blue shift of the eigenmodes due to vertical confinement in the planar waveguide. This effect, which is more pronounced for slabs with strong out-of-plane refractive index contrast, implies that the frequencies of photonic bands and gaps depend on all parameters of the planar waveguide (layer thicknesses and refractive indices) and can differ substantially from those of the reference 1D or 2D system. Finally, the eigenmodes of photonic crystal slabs can be put in one-to-one correspondence with those of the reference system only when the frequency is sufficiently low for the waveguide to be monomode. The cut-off frequency of second- and higher-order modes also depends on slab parameters and on the photonic lattice.

In this work we present a systematic study of photonic bands, gap maps and diffraction losses for 1D photonic crystal slabs, that is 1D photonic lattices like those of a distributed Bragg reflector (see Fig. 1a for the 1D reference system). These are defined in two types of waveguides with strong refractive index contrast: the self-standing membrane or *air bridge* (Fig. 1b) and the asymmetric photonic crystal slab in which only the core layer is patterned (Fig. 1c). The latter structure is typi-

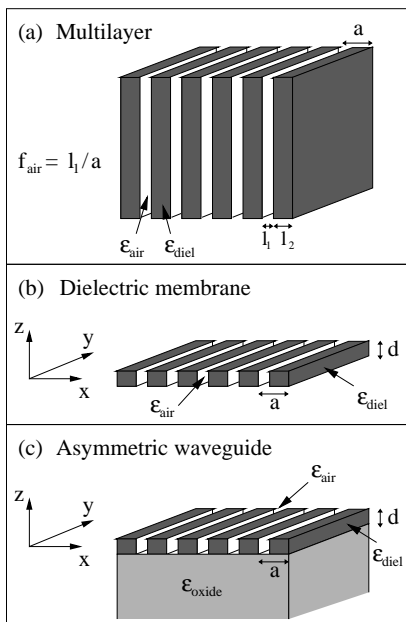


FIG. 1: Photonic structures studied in this work: (a) Ideal one-dimensional photonic crystal, with period  $a$  and air fraction  $f_{\text{air}} = l_1/a$ . (b) Photonic crystal slab consisting of a self-standing, patterned dielectric core (*air bridge* or *membrane*) of thickness  $d$  surrounded by air. (c) Photonic crystal slab, with the pattern defined in a high-index dielectric core of thickness  $d$  sandwiched between air and an insulating oxide substrate. Throughout this work we assume:  $\epsilon_{\text{diel}} = 12$ ,  $\epsilon_{\text{oxide}} = 2.1$ ,  $\epsilon_{\text{air}} = 1$ .

cally realized with the Silicon-on-Insulator (SOI) system but may also be realized with GaAs on an oxide layer. We assume the following values of the dielectric constants:  $\epsilon_{\text{diel}} = 12$  for the high-index core layer (as appropriate to Si or GaAs below the band gap),  $\epsilon_{\text{air}} = 1$ , and  $\epsilon_{\text{oxide}} = 2.1$  (as appropriate for  $\text{SiO}_2$  or other oxides). The periodic patterning is taken along the  $x$  direction and throughout this paper we assume  $k_y = 0$ . The gap maps are calculated as a function of air fraction in the core layer and for different values of the core thickness, thereby exploring a wide range of parameters of experimental interest. The dependence of the radiation losses on frequency, polarization, and air fraction is also calculated and discussed.

The photonic bands and gap maps of a distributed Bragg reflector are obviously well known and are exemplified in Fig. 2.<sup>43</sup> Notice that the photonic bands of Fig. 2a (which refer to an air fraction  $f_{\text{air}} = 0.3$ ) as well as the gap map of Fig. 2b are degenerate for transverse electric (TE) and transverse magnetic (TM) polarizations with respect to the plane of incidence: this degeneracy is lifted in a waveguide because the confinement-induced shift is polarization-dependent, as was already shown experimentally.<sup>35</sup> One of the goals of the present paper is to establish whether a complete band gap for both polarizations can occur in a waveguide-embedded 1D photonic structure.

Related concepts have been studied in the context of dielectric waveguide gratings, also called resonant grating filters.<sup>41,44–59</sup> These kinds of diffraction gratings may support guided and leaky modes. The latter are resonantly coupled to an external light beam and give rise to narrow resonances in reflection or transmission, which may be used for polarization-dependent filters<sup>44</sup> or for enhanced nonlinear optical effects.<sup>47,56</sup> Most of the research concentrated on systems with a weak dielectric modulation, e.g., surface relief gratings for filtering and distributed feedback,<sup>41,46</sup> waveguides with a weak refractive index contrast within the core region<sup>45,48,50</sup> and/or which are modeled by a single Fourier component of the dielectric function.<sup>44,51–53,58</sup> For an extensive list of previous literature along these lines and of the different kinds of theoretical methods used we refer to the book by Loewen and Popov.<sup>49</sup> In all these cases, which can be treated at least qualitatively by coupled-mode theory, the dispersion of the waveguide mode is only weakly modified by the dielectric modulation and photonic bandgap effects are very small. Specific waveguide grating structures with strong refractive index modulation in the plane leading to an appreciable photonic gap have been studied in Refs. 54,55 for the case of TE polarization, and in Refs. 57,59 for both TE and TM polarizations. In these strongly modulated cases a rigorous coupled-wave analysis (also called the Fourier modal method) is necessary and has been used. We point out that the focus of the present work is quite different from all these papers, in particular for what concerns the systematic calculation of gap maps and losses as a function of frequency and of various structure parameters.

This work is organized as follows. In Sec. II we give a short description of the theoretical method for calculating photonic bands and intrinsic losses in a waveguide. In Sec. III we discuss a few examples of photonic mode dis-

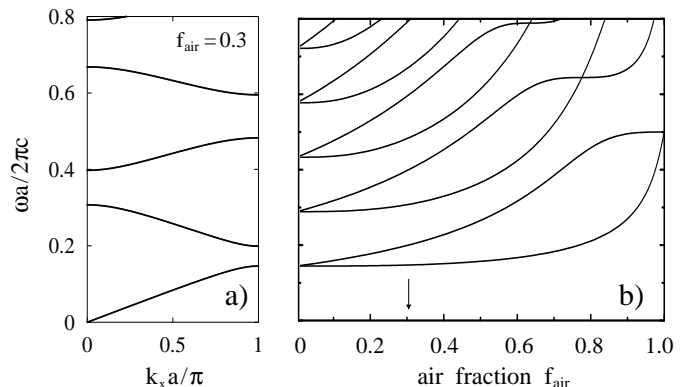


FIG. 2: Ideal multilayer: (a) Photonic bands for  $f_{\text{air}} = 0.3$ ; TE and TM modes are exactly degenerate. (b) Gap map, i.e., band edges as a function of air fraction; the value of  $f_{\text{air}}$  corresponding to the calculation given in (a) is indicated by an arrow.

persion, both for symmetric and asymmetric 1D photonic crystal slabs. Section IV contains detailed results for 1D gap maps in a membrane or in an asymmetric waveguide for different values of the core thickness. In Sec. V we present results for intrinsic losses of quasi-guided modes. In Sec. VI we give a few closing remarks.

## II. METHOD

The approach adopted here, which was already introduced in Refs. 36,37, relies on a finite-basis expansion in order to transform the second-order equation for the magnetic field in a linear eigenvalue problem. The basis consists of the guided modes of an effective homogeneous waveguide, where the dielectric constant of each layer is defined by the spatial average of the dielectric constant  $\epsilon(\mathbf{r})$  over the photonic pattern. The in-plane Bloch vector  $\mathbf{k}$  is obviously conserved modulo a reciprocal lattice vector  $\mathbf{G}$ . The off-diagonal components  $\epsilon_{\mathbf{G},\mathbf{G}'}$  of the dielectric tensor give rise to band splittings and to a folding of the photonic modes in the first Brillouin zone. Some of the photonic modes may lie below the cladding light line and be truly guided, however most (sometimes all) of them fall above the light line in the first Brillouin zone. Coupling of these modes to leaky modes of the effective waveguide is taken into account by time-dependent perturbation theory, which leads to an expression for the imaginary part of the mode frequency in terms of the photonic density of states at fixed in-plane wavevector.<sup>23,37,60</sup> This procedure is formally analogous to Fermi's golden rule in quantum mechanics. When the waveguide is asymmetric (like in the case of the SOI structure), care must be taken to express the leaky modes in terms of outgoing states and to relate them to the respective state densities.<sup>61</sup>

The approximations made in the present approach are as follows (for a fuller discussion see Refs. 36,37). The effective dielectric constant of the homogeneous waveguide, which defines the basis of guided modes for the expansion, is chosen to be

$$\epsilon_{\text{eff}} = f_{\text{air}}\epsilon_{\text{air}} + (1 - f_{\text{air}})\epsilon_{\text{diel}}, \quad (1)$$

for both TE and TM polarizations. This choice is by no means unique, although it is the exact definition of the effective dielectric constant for TE polarization and anyway when the electric field is perpendicular to the direction of periodicity.<sup>62</sup> For TM-polarized modes, which have electric field components along  $x$  and  $z$ , the situation is more complex.<sup>63</sup> It is known from the literature that the  $x$  component of the electric field is subject to an effective dielectric constant that is obtained from the inverse averaging rule,<sup>62</sup> therefore a different choice of  $\epsilon_{\text{eff}}$  in the patterned region could be suggested for TM modes. Choices of  $\epsilon_{\text{eff}}$  differing from Eq. (1) do not lead to any appreciable change of the results above the mode cutoff, as we have verified. The frequency position of the cutoff does depend on the choice of  $\epsilon_{\text{eff}}$ , especially for large

air fractions, however a comparison with exact scattering matrix calculations<sup>35,36</sup> shows that the average dielectric constant defined by Eq. (1) gives very good agreement with the frequencies and cutoff positions obtained from the exact calculations. It should also be noted that the electromagnetic field close to mode cutoff is mostly extended in the claddings, where the dielectric constants are homogeneous for the airbridge and SOI structures studied in the present paper.

The number of reciprocal lattice vectors  $\mathbf{G}$  is limited by a finite cut-off, like for usual plane-wave calculations,<sup>64</sup> and in addition a restricted number of guided modes of the effective waveguide is kept in the expansion. For the calculations shown in this work, a number of 31 plane waves is usually taken in the basis set and is sufficient for convergence with better than percent accuracy. The number of guided modes in the expansion is not found to be critical in the energy range considered and is usually taken to be  $\leq 8$ . For the quasi-guided modes, neglect of the second-order shift due to coupling to leaky modes introduces an error of less than a few percent in the photonic frequencies. All these approximations are justified *a posteriori* by the close agreement of the calculated photonic frequencies with those obtained from reflectivity calculations<sup>36</sup> made with the exact scattering-matrix method.<sup>9</sup> Finally, calculating the radiative losses of quasi-guided modes by first-order perturbation theory is justified by the fact that the imaginary part of the frequency is much smaller than the real part, as shown by the results below.

## III. PHOTONIC BANDS

The photonic bands of the strong confinement symmetric slab, corresponding to the system schematically shown in Fig. 1b, are displayed in Fig. 3b and 3c for a core thickness  $d = 0.4a$  and an air fraction  $f_{\text{air}} = 0.3$ . The bands are plotted by using dimensionless frequency  $\omega a / (2\pi c) = a / \lambda$  as a function of in-plane wave vector  $k_x a / \pi$  in the first Brillouin zone. The photonic dispersion curves of the patterned structure are compared to those of a uniform dielectric slab suspended in air (Figs. 3a and 3d) with a spatially averaged dielectric constant given by Eq. (1), that is  $\epsilon_{\text{eff}} = 8.7$  in the present case. The guided modes of Figs. 3a and 3d represent the basis set for the expansion method discussed in the previous Section. The dispersion for the average dielectric slab is presented in the reduced zone scheme, allowing for a direct comparison with the corresponding photonic bands of the patterned waveguide. We have classified the guided modes according to mirror symmetry with respect to the plane of incidence  $\mathbf{k}z \equiv xz$  (we use  $\sigma_{xz}$  to denote this operation) and with respect to the  $xy$  plane ( $\sigma_{xy}$  operation). The modes whose electric field component lies in the  $xy$  plane are referred to as TE, and are odd with respect to specular reflection through the plane of incidence ( $\sigma_{xz} = -1$ ); the modes whose magnetic field lies in the

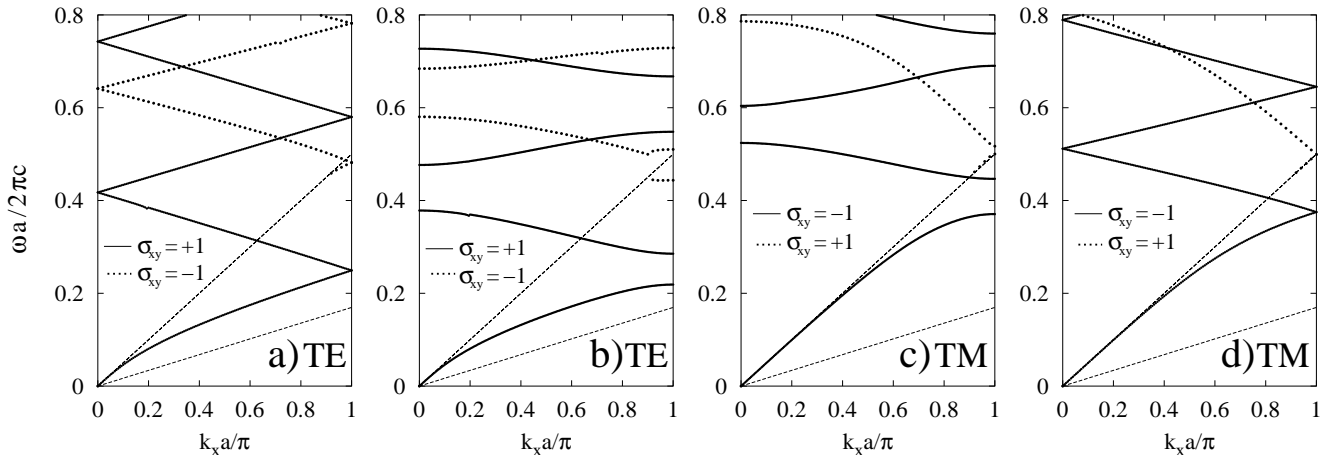


FIG. 3: Photonic bands for the membrane structure of Fig. 1b. The dashed lines represent the dispersions of light in air and in the average core layer. (a) TE, (d) TM dispersion curves, folded in the first Brillouin zone, for a uniform dielectric membrane with  $\epsilon_{\text{eff}} = 8.7$  and thickness  $d/a = 0.4$ ; (b) TE, (c) TM photonic bands for the patterned structure with  $f_{\text{air}} = 0.3$ ,  $d/a = 0.4$ .

$xy$  plane are labelled as TM and are even with respect to mirror plane  $xz$  ( $\sigma_{xz} = +1$ ).<sup>22</sup> These modes can be classified further as even ( $\sigma_{xy} = +1$ ) or odd ( $\sigma_{xy} = -1$ ) with respect to specular reflection through the  $xy$  plane, thus giving four different types of guided eigenfunctions for the electromagnetic field. We can separately compare Fig. 3a to 3b and Fig. 3c to 3d. It is clearly seen that for both TE and TM modes the periodic patterning of the dielectric slab introduces band gaps around the degenerate points of the average slab dispersion curves ( $k_x = 0$  and  $k_x = \pm\pi/a$ ), owing to the off-diagonal components of the inverse dielectric tensor. There is one-to-one correspondence between average slab and 1D PC slab modes. The first-order modes (TE even and TM odd) have no cut-off frequency, as is well known for a symmetric waveguide. The second-order guided modes have a finite cut-off frequency, which is degenerate for TE and TM modes. The second-order mode, represented by dotted lines, has  $\sigma_{xy} = -1$  for TE polarization, while it has  $\sigma_{xy} = +1$  for TM polarization.

A second point should be remarked by comparing the photonic bands of Figs. 3b and 3c to the bands of an ideal multilayer. The first photonic band gap appears between 0.15 and 0.20 in the ideal 1D case, and between 0.22 and 0.28 for the lowest TE mode in the PC slab, due to the confinement effect along the vertical ( $z$ ) direction. The gap between the first and the second band opens between 0.37 and 0.45 when considering TM modes: these values are strongly blue shifted with respect to both the multilayer and the TE modes of the PC slab. Thus the confinement effect manifests itself in the blue shift of the eigenfrequencies of the electromagnetic field with respect to the ideal multilayer, and moreover in the removal of degeneracy between TE and TM modes: the latter effect is due to the stronger confinement of TM compared to TE modes in the planar waveguide.<sup>41</sup> We also notice

that all the band gaps, except for the first one, lie in the region of guided resonances, and could be experimentally tested by external reflectance measurements. The first band gap, either TE even or TM odd, is instead in the region of truly guided modes. A complete band gap common to both polarizations can also be seen around  $\omega a/(2\pi c) \sim 0.4$ , where the second-order TE gap overlaps the first-order TM gap. As we will see in the next section, this is rather a coincidence for 1D PC slabs.

In Fig. 4 we display the photonic bands for the asymmetric structure represented in Fig. 1c. The dashed lines are the dispersions of photons in air, substrate and effective dielectric core. The parameters used in these cal-

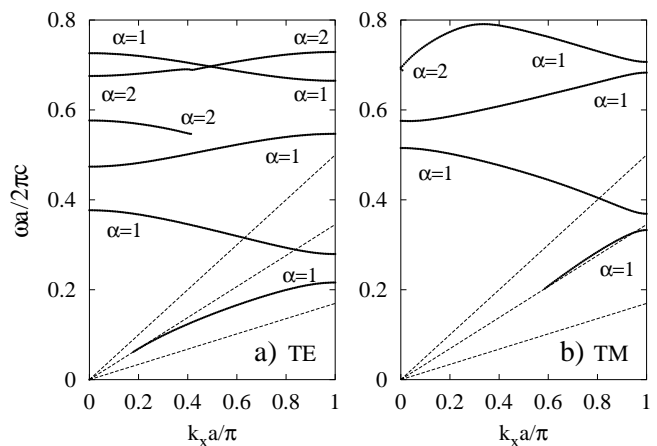


FIG. 4: Photonic bands for the patterned dielectric-on-insulator structure of Fig. 1c with  $f_{\text{air}} = 0.3$ ,  $d/a = 0.4$ . The dashed lines are the light dispersions in the effective core and in the upper and lower claddings;  $\alpha$  labels the order of the guided mode. (a) TE, (b) TM modes.

culations are  $d/a = 0.4$ ,  $f_{\text{air}} = 0.3$ , allowing for a direct comparison with the results of Figs. 3b and 3c. Owing to the asymmetry of the vertical waveguide,  $\sigma_{xy}$  is no more a symmetry operation: the modes can only be classified as odd (TE, Fig. 4a) or even (TM, Fig. 4b) with respect to the plane of incidence. However, we have indicated the approximate order of the waveguide mode by the index  $\alpha$  in Fig. 4 (this can be defined only when the modes are well separated in frequency, otherwise mixing and anticrossing effects occur). For an asymmetric slab there are no modes starting at  $\omega = 0$ .<sup>41</sup> By comparing Figs. 3 and 4, we notice that the lowest TE mode of the asymmetric 1D PC slab is in quantitative agreement with the first-order TE mode of the PC membrane; instead, the TM modes of the asymmetric slab are somewhat less confined than those of the PC membrane. It is important to stress that the modes lying between the two claddings light lines (oxide and air in this case) are evanescent in air, but leaky in the substrate. These modes have finite radiative losses, as we will see in section V. We also notice that no complete band gap is present in the asymmetric 1D PC slab, at variance with the corresponding symmetric structure. The results shown in Fig. 4 are conceptually similar to Brillouin diagrams calculated for TE polarization in the case of an asymmetric waveguide grating structure.<sup>55</sup> We point out that the described features of photonic band structures for an asymmetric 1D PC slab were experimentally verified by variable angle surface reflectance performed on SOI structures, for both TE and TM modes.<sup>35</sup>

#### IV. GAP MAPS

In this section we present a complete set of gap maps for waveguide-embedded 1D photonic crystals. We consider a *band gap* as a frequency region where no photonic modes exist, either truly guided or quasi-guided above the light line. We present the gap maps for modes with TE or TM polarizations, i.e., with definite parity with respect to the vertical mirror symmetry  $\sigma_{xz}$ : this convention applies to symmetric as well as asymmetric vertical waveguide structures. For the case of the asymmetric structure, for which the lowest-order waveguide mode has a finite cut-off, only the frequency region above the lowest-order cut-off is physically relevant.

##### A. Dielectric membrane

In Fig. 5 we display the calculated gap maps for the air bridge structure of Fig. 1b. We show the maps for three different slab thicknesses, namely  $d/a = 0.2, 0.4, \text{ and } 0.8$ . We display in black the true complete band gap, i.e., the frequency region in which no photonic modes (or resonances) are allowed for any polarization. The gap maps are shown for air fraction varying from 0 to 0.7, which represent a realistic range for practical realization.

The solid lines in Fig. 5 represent the cut-off frequency of the second-order waveguide mode, which is given by

$$\frac{\omega_c a}{2\pi c} = \frac{a}{2d\sqrt{\epsilon_{\text{eff}} - \epsilon_{\text{air}}}} \quad (2)$$

and is the same for both polarizations.

An important feature that we can see from Fig. 5 is that for  $d/a = 0.2$ , the TE gap map is qualitatively similar to the ideal multilayer one (see Fig. 2b) with a blue shift arising from the confinement effect. The band gaps for TM modes are shifted to much higher frequencies and some complete band gaps start to appear only at  $a/\lambda \sim 0.7$ . The gap map is more complex for  $d/a = 0.4$ , due to the appearance of higher-order waveguide modes at low frequency. Nevertheless, for  $a/\lambda \lesssim 0.4$  the slab is still monomode, and a large complete band gap opens in a wide range of air fractions (Fig. 5b). This complete gap comes from the overlap of the first TM gap (at the Brillouin zone edge, see Fig. 3c) and the second TE one (at the zone center, Fig. 3b). No complete band gap has been found for other values of  $d/a$  (calculations not shown). For  $d/a = 0.8$  the photonic band structure is quite complex because the slab becomes multimode already at low frequencies. The band gap in TM modes is still present around  $a/\lambda \sim 0.4$ , but no complete band gap exists because of the presence of second-order TE modes. The conclusions from these results are the following: (i) the TE gap map in a waveguide resembles the ideal 1D one only below the cut-off of second-order modes, (ii) the TM gap map is very sensitive to the structure parameters, and (iii) a complete gap for both polarizations is calculated to occur only for a core thickness around  $d/a = 0.4$ .

##### B. Asymmetric waveguide

In Fig. 6 we show the calculated gap maps of the asymmetric 1D PC slab of Fig. 1c, for core thicknesses  $d/a = 0.2, 0.4, \text{ and } 0.8$ . The gap maps of Fig. 6 show notable differences as compared to those of the PC membrane.

One of the peculiarities of the asymmetric structure is the existence of a finite cut-off frequency for the lowest-order TE and TM modes. The cut-off frequency as a function of air fraction is plotted with dashed lines for TE modes, and with solid lines for TM modes. The values for the cut-off frequencies obtained by the present approach coincide with those following from the expression for a uniform, asymmetric slab. The formula is<sup>41</sup>

$$\frac{\omega_c a}{2\pi c} = \frac{a}{2d\sqrt{\epsilon_{\text{eff}} - \epsilon_{\text{oxide}}}} \left[ m + \frac{1}{\pi} \arctan \left( r \frac{\sqrt{\epsilon_{\text{oxide}} - \epsilon_{\text{air}}}}{\sqrt{\epsilon_{\text{eff}} - \epsilon_{\text{oxide}}}} \right) \right] \quad (3)$$

where  $r = 1$  for TE modes,  $r = \epsilon_{\text{eff}}/\epsilon_{\text{air}}$  for TM modes, and  $m \geq 0$  is an integer.

For  $d/a = 0.2$  the asymmetric 1D PC slab has only first-order TE and TM modes in the whole frequency

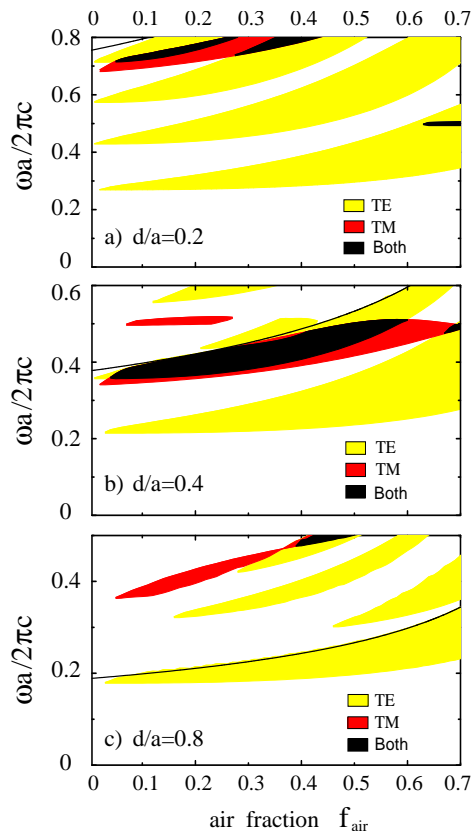


FIG. 5: Gap maps for the membrane structure of Fig. 1b, as a function of the air fraction  $f_{\text{air}} = l_1/a$ . Solid lines represent the cut-off frequency of the second-order waveguide mode. (a) Core thickness  $d/a = 0.2$ , (b)  $d/a = 0.4$ , (c)  $d/a = 0.8$ .

range shown. The TE band gaps are again qualitatively similar to those of the ideal 1D multilayer, with a confinement effect which is close to that of the membrane case (Fig. 5a); the TM gaps are instead shifted to much higher frequencies as compared to the 1D multilayer. The first TE band gap is in a region below the cut-off of the first-order TM mode, thus it may be considered as a complete band gap. For  $d/a = 0.4$  and  $0.8$  a second-order TE cut-off appears at frequencies around  $0.44$  and  $0.22$ , respectively: the TE gap map is similar to that of the 1D multilayer only below the second-order cut-off frequency. The TM gaps are always very different from those of the ideal 1D case and also quite different from those of the PC membrane: TM modes are seen to be extremely sensitive to the structure parameters (core thickness and claddings dielectric constants). As it can be seen by comparing Figs. 5b and 6b, the complete band gap for  $d/a = 0.4$  occurs for the particular case of a 1D PC membrane but not in the asymmetric PC slab. For  $d/a = 0.8$  a complete band gap resulting from the overlap of the first TE and TM gaps appears around  $a/\lambda \sim 0.3$  for  $f_{\text{air}} \gtrsim 0.5$ .

As a general remark, the numerical results for photonic bands and gaps previously shown relate only to the real part of the frequency and do not consider the ef-

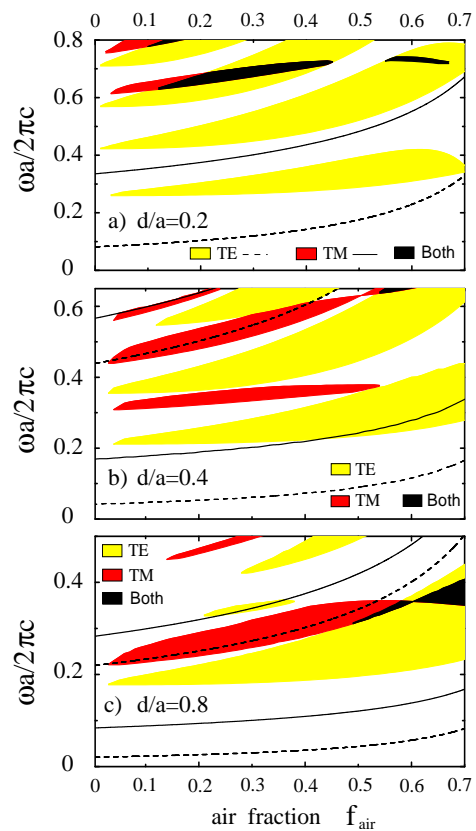


FIG. 6: Gap maps for the asymmetric PC slab structure of Fig. 1c. Dashed (solid) lines represent the cut-off frequencies of the first- and second-order waveguide modes for TE (TM) polarization. (a) Core thickness  $d/a = 0.2$ , (b)  $d/a = 0.4$ , (c)  $d/a = 0.8$ .

fect of coupling to radiative waveguide modes. Thus the physical relevance of a photonic band dispersion is expected to decrease on increasing the frequency far from the light line. We also notice that the concept of mode cut-off for resonant modes is not clearly defined when radiative broadening is taken into account. For these reasons, the gap maps calculated here are expected to be more useful in the low frequency region, in particular for the band gaps which open below the second-order cut-off lines shown in Figs. 5 and 6.

## V. DIFFRACTION LOSSES

To complete our analysis of 1D PC slabs we have to address also the imaginary part of frequency, which gives information about the radiative losses due to out-of-plane diffraction. This is done by using time-dependent perturbation theory for the electromagnetic problem, as previously discussed in Section II. We display in Fig. 7 the results for parameters  $d/a = 0.2$  and  $f_{\text{air}} = 0.3$ , for both a PC membrane and an asymmetric PC slab. In Figs. 7a and 7b the band diagram and the corresponding imag-

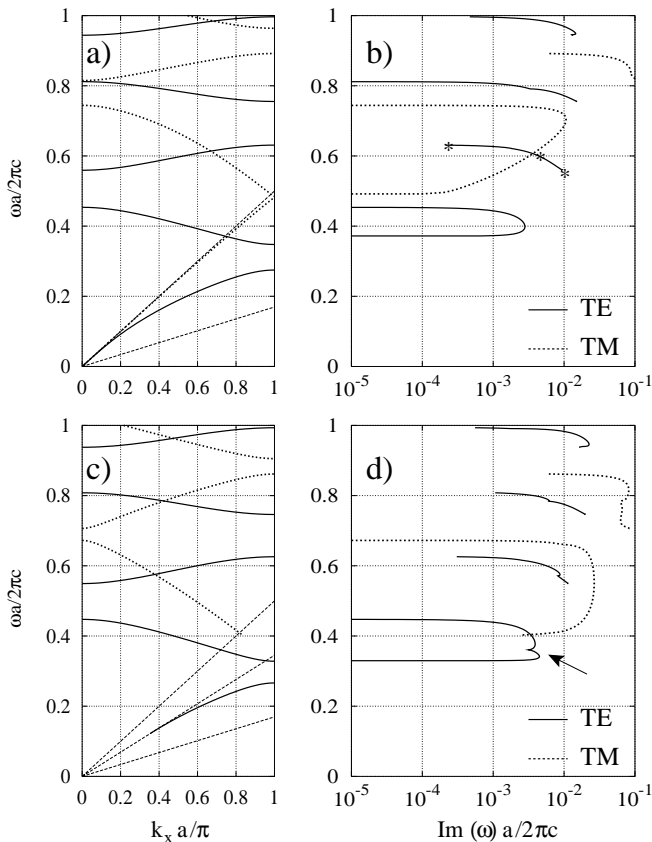


FIG. 7: (a) Photonic bands and (b) imaginary part of frequency for a symmetric 1D PC membrane; (c) photonic bands and (d) imaginary part of frequency for an asymmetric 1D PC slab. Parameters are  $d/a = 0.2$ ,  $f_{\text{air}} = 0.3$ . Solid (dashed) lines are TE (TM) modes. The three markers in (b) correspond to the points marked in Fig. 8 (see text). The arrow in (d) denotes the cusp, which corresponds to the second TE band in (c) crossing the air light line.

inary part of frequencies are shown for the symmetric 1D PC slab. In Fig. 7a the waveguide is monomode for both TE and TM polarizations. In Fig. 7b we show the dimensionless quantity  $\text{Im}(\omega)a/(2\pi c)$ , corresponding to each photonic band of Fig. 7a, as a function of mode frequency. The imaginary part is generally much smaller than the real part, indicating the validity of the perturbative treatment adopted. The losses go to zero when the mode crosses the light line in air and becomes truly guided. It is clear from the figure that the radiative losses generally increase on increasing the photonic band index, however the behavior of the losses within a given photonic band is nontrivial and has to be studied in each specific case. The guided resonances at the Brillouin zone center present a quite interesting behavior. In fact, the second and the fourth TE bands have zero linewidth at  $k_x = 0$  (their frequencies are  $\omega a / (2\pi c) = 0.45$  and  $0.81$ , respectively) while the third and the fifth band have finite radiative widths at  $k_x = 0$  ( $\omega a / (2\pi c) = 0.56$  and  $0.94$ ).

A similar behavior holds also for TM modes. These numerical results could be probed by variable angle surface reflectance experiments made on 1D PC membranes: the imaginary part of the frequency can be extracted from the linewidth of spectral structures in reflectance that correspond to photonic modes.<sup>14,20</sup>

In Figs. 7c and 7d we show the results for an asymmetric 1D PC slab with the same thickness and air fraction.<sup>65</sup> The radiative losses shown in Fig. 7d display quite the same behavior as in the membrane case. They are about two times larger than the corresponding losses of Fig. 7b: this is due to the asymmetry of the vertical waveguide, which implies that a quasi-guided mode above the light line is coupled to all radiative modes of the effective waveguide at the same frequency, without the parity selection rule which holds instead in the symmetric case. A similar behavior was found in the calculation of spectral properties of deep 1D gratings.<sup>17</sup> Moreover, the higher-order modes (either TE or TM) now have a finite  $\text{Im}(\omega)$  also at  $k_x = 0$ : this is due to the additional diffraction channels for radiative losses which are present in the asymmetric waveguide. Moreover, we notice that the modes whose frequencies lie between the light lines of air and oxide claddings are not truly guided, i.e., they are evanescent in air but leaky in the substrate. Thus, the crossing between a band and the light line in air does not cause the linewidth of the photonic resonance to go to zero: rather,  $\text{Im}(\omega)$  has a cusp (marked by an arrow in Fig. 7d) when the light line in air is crossed. Similar features can be recognized in Fig. 7d at higher frequencies: they arise whenever a photonic mode crosses a cladding light line folded in the first Brillouin zone. These notable features of  $\text{Im}(\omega)$  are not a numerical artifact, but rather

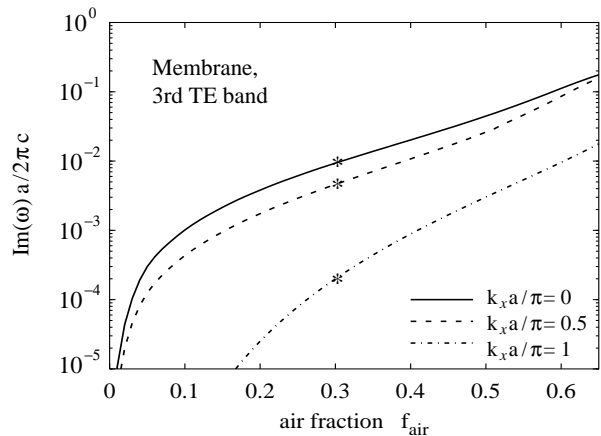


FIG. 8: Imaginary part of photonic frequencies as a function of the air fraction for the PC membrane of thickness  $d/a = 0.2$ ; the three curves correspond to different wavevectors ( $k_x = 0$ ,  $k_x = \pi/2a$ ,  $k_x = \pi/a$ ) in the first Brillouin zone of the third TE photonic band. The three points marked on the curves correspond to the three markers of Fig. 7b, where  $f_{\text{air}} = 0.3$ .

they correspond physically to the opening or closing of diffraction channels for radiative losses.

We also found that the imaginary part of frequency increases on increasing the air fraction in the investigated range, as shown in Fig. 8, where  $\text{Im}(\omega a/2\pi c)$  is plotted for the PC membrane of thickness  $d/a = 0.2$ . A similar behavior is found also for the asymmetric structure (not shown here) and an increase of the photonic mode linewidth with the air fraction was already stated experimentally.<sup>21,35</sup> The three curves of Fig. 8 correspond to the evolution of the losses for the third TE photonic band at three different points in the first Brillouin zone. When  $f_{air} = 0.3$  the corresponding photonic band has frequencies around  $\omega a/(2\pi c) = 0.6$  (see Fig. 7a), and the three points marked in Fig. 8 correspond to those marked in Fig. 7b. Notice that the losses vary in a logarithmic scale and become extremely small either towards the homogeneous waveguide limit at low air fraction or close to the Brillouin zone edge. While the filling fraction dependence of the losses is similar for all bands and polarizations, the wavevector dependence changes from band to band, as it appears from Figs. 7b,d. It can be concluded that for the present waveguide-embedded 1D photonic structures, the spectral linewidth of quasi-guided photonic modes can vary by several orders of magnitude and it depends in a nontrivial way on the structure parameters as well as on the angle of incidence, mode index, and polarization.

## VI. CONCLUSIONS

We have studied the photonic bands and the gap maps of one-dimensional photonic crystal slabs made of a high refractive index material sandwiched between low index claddings, thus providing strong confinement of electromagnetic waves along the vertical direction. The method adopted yields the frequencies of photonic modes both below and above the light line, and therefore allows treating guided and quasi-guided modes on the same footing.

Photonic modes in a 1D photonic crystal waveguide can be put in one-to-one correspondence with those of

the ideal 1D reference system only when the waveguide is monomode. Under this condition, the TE gap maps are qualitatively similar to the ideal 1D ones considering the blue shift in the waveguide. This confinement effect is considerably more pronounced for TM-polarized than for TE-polarized modes, thereby leading to a polarization splitting which depends in a sensitive way on the structure parameters. As a consequence, a complete band gap common to TE and TM polarizations is generally not found in 1D photonic crystal slabs, except for special values of the parameters.

The radiative losses of guided resonances due to out-of-plane diffraction depend in a sensitive way on waveguide parameters, mode index, and frequency. For some modes the imaginary part of the frequency vanishes at the Brillouin zone center, thus even above the light line it is possible to find photonic modes with very low losses. In general, the losses are predicted to be higher for Silicon-on-Insulator structures as compared to photonic crystal membranes, due to the asymmetry of the planar waveguide. All these results are related to the presence of diffraction channels for radiative couplings.

The quantitative results for the complex frequency dispersion of quasi-guided modes may be experimentally tested by performing reflectance or transmittance measurements with light incident on the PC slab surface. Modes below the light line can be probed in waveguide transmission experiments. Moreover, the results of the present work may be useful for designing 1D PC slabs with gaps at specified frequencies, regions of monomode propagation, and low diffraction losses. They might also be used for the design of advanced 1D structures like filters and microcavities. The same theoretical approach can be applied to PC slabs with various 2D patterns.

## Acknowledgments

The authors are grateful to M. Agio, M. Galli and M. Patrini for several helpful discussions. This work was supported by MIUR through Cofin and FIRB programs and by INFN through PRA PHOTONIC.

<sup>1</sup> For recent reviews, see e.g. papers in IEEE J. Quantum Electron. **38**, Feature Section on Photonic Crystal Structures and Applications, edited by T.F. Krauss and T. Baba, pp. 724-963 (2002).

<sup>2</sup> T.F. Krauss, R.M. De La Rue, and S. Brand, Nature **383**, 699 (1996).

<sup>3</sup> S. Fan, P.R. Villeneuve, J.D. Joannopoulos, and E.F. Schubert, Phys. Rev. Lett. **78**, 3294 (1997).

<sup>4</sup> D. Labilloy, H. Benisty, C. Weisbuch, T.F. Krauss, R.M. De La Rue, V. Bardinal, R. Houdré, U. Oesterle, D. Cassagne, and C. Jouanin, Phys. Rev. Lett. **79**, 4147 (1997).

<sup>5</sup> T. Fujita, Y. Sato, T. Kuitani, and T. Ishihara, Phys. Rev. B **57**, 12428 (1998).

<sup>6</sup> H. Benisty, C. Weisbuch, D. Labilloy, M. Rattier, C.J.M. Smith, T.F. Krauss, R.M. De La Rue, R. Houdré, U. Oesterle, C. Jouanin, and D. Cassagne, J. Light-wave Technol. **17**, 2063 (1999).

<sup>7</sup> S.G. Johnson, S. Fan, P.R. Villeneuve, J.D. Joannopoulos, and L.A. Kolodziejski, Phys. Rev. B **60**, 5751 (1999).

<sup>8</sup> V.N. Astratov, D.M. Whittaker, I.S. Culshaw, R.M. Stevenson, M.S. Skolnick, T.F. Krauss, and R.M. De La Rue, Phys. Rev. B **60**, R16255 (1999).

<sup>9</sup> D.M. Whittaker and I.S. Culshaw, Phys. Rev. B **60**, 2610 (1999).

<sup>10</sup> H. Benisty, D. Labilloy, C. Weisbuch, C.J.M. Smith, T.F. Krauss, D. Cassagne, A. Béraud, and C. Jouanin,

- Appl. Phys. Lett. **76**, 532 (2000).
- 11 T. Søndergaard, A. Bjarklev, M. Kristensen, J. Erland, and J. Broeng, Appl. Phys. Lett. **77**, 785 (2000).
  - 12 E. Silvestre, J.M. Pottage, P.S. Russel, and P.J. Roberts, Appl. Phys. Lett. **77**, 942 (2000).
  - 13 M. Lončar, D. Nedeljković, T. Doll, J. Vučković, A. Scherer, and T. P. Pearsall, Appl. Phys. Lett. **77**, 1937 (2000).
  - 14 V. Pacradouni, W.J. Mandeville, A.R. Cowan, P. Paddon, J.F. Young, and S.R. Johnson, Phys. Rev. B **62**, 4204 (2000).
  - 15 A. Chutinan and S. Noda, Phys. Rev. B **62**, 4488 (2000).
  - 16 E. Chow, S.Y. Lin, S.G. Johnson, P.R. Villeneuve, J.D. Joannopoulos, J. R. Wendt, G.A. Vawter, W. Zubrzycki, H. Hou, and A. Alleman, Nature **407**, 983 (2000).
  - 17 J. Čtyroký, J. Opt. Soc. Am. A **18**, 435 (2001).
  - 18 P. Lalanne and H. Benisty, J. Appl. Phys. **89**, 1512 (2001).
  - 19 M. Palamaru and P. Lalanne, Appl. Phys. Lett. **78**, 1466 (2001).
  - 20 A.R. Cowan, P. Paddon, V. Pacradouni, and J. Young, J. Opt. Soc. Am. A **18**, 1160 (2001).
  - 21 N. Kawai, K. Inoue, N. Carlsson, N. Ikeda, Y. Sugimoto, K. Asakawa, and T. Takemori, Phys. Rev. Lett. **86**, 2289 (2001).
  - 22 T. Ochiai and K. Sakoda, Phys. Rev. B **63**, 125107 (2001).
  - 23 T. Ochiai and K. Sakoda, Phys. Rev. B **64**, 045108 (2001).
  - 24 K. Sakoda, *Optical Properties of Photonic Crystals* (Springer, Berlin, 2001).
  - 25 D.M. Whittaker, I.S. Culshaw, V.N. Astratov, and M.S. Skolnick, Phys. Rev. B **65**, 073102 (2002).
  - 26 M. Lončar, D. Nedeljković, T.P. Pearsall, J. Vučković, A. Scherer, S. Kuchinsky, and D.C. Allan, Appl. Phys. Lett. **80**, 1689 (2002).
  - 27 G.R. Hadley, IEEE Photon. Technol. Lett. **14**, 642 (2002).
  - 28 S. Fan and J.D. Joannopoulos, Phys. Rev. B **65**, 235112 (2002).
  - 29 S.G. Tikhodeev, A.L. Yablonskii, E.A. Muljarov, N.A. Gippius, and T. Ishihara, Phys. Rev. B **66**, 045102 (2002).
  - 30 M. Galli, M. Agio, L.C. Andreani, L. Atzeni, D. Bajoni, G. Guizzetti, L. Businaro, E. Di Fabrizio, F. Romanato, and A. Passaseo, Eur. Phys. J. B **27**, 79 (2002).
  - 31 M. Qiu, Phys. Rev. B **66**, 033103 (2002).
  - 32 D. Peyrade, E. Silberstein, P. Lalanne, A. Talneau, and Y. Chen, Appl. Phys. Lett. **81**, 829 (2002).
  - 33 D. Peyrade, Y. Chen, A. Talneau, M. Patrini, M. Galli, F. Marabelli, M. Agio, L.C. Andreani, E. Silberstein, and P. Lalanne, Microelectron. Engin. **61** – **62**, 529 (2002).
  - 34 A.D. Bristow, V.N. Astratov, R. Shimada, I.S. Culshaw, M.S. Skolnick, D.M. Whittaker, A. Tahraoui, and T.F. Krauss, IEEE J. Quantum Electron. **38**, 880 (2002).
  - 35 M. Patrini, M. Galli, F. Marabelli, M. Agio, L.C. Andreani, D. Peyrade, and Y. Chen, IEEE J. Quantum Electron. **38**, 885 (2002).
  - 36 L.C. Andreani and M. Agio, IEEE J. Quantum Electron. **38**, 891 (2002).
  - 37 L.C. Andreani, Physica Status Solidi (b) **234**, 139 (2002).
  - 38 L.C. Andreani and M. Agio, Appl. Phys. Lett. **82**, 2011 (2003).
  - 39 K. Koshino, Phys. Rev. B **67**, 165213 (2003).
  - 40 A.D. Bristow, D.M. Whittaker, V.N. Astratov, M.S. Skolnick, A. Tahraoui, T.F. Krauss, M. Hopkinson, M.P. Croucher, and G.A. Gehring, Phys. Rev. B **68**, 033303 (2003).
  - 41 A. Yariv and P. Yeh, *Optical Waves in Crystals* (Wiley, New York, 1984).
  - 42 J.D. Joannopoulos, R.D. Meade, and J.N. Winn, *Photonic Crystals: Molding the Flow of Light* (Princeton University Press, Princeton, 1995).
  - 43 For  $\epsilon_{\text{diel}} = 12$  the  $\lambda/4$  condition occurs at  $f_{\text{air}} = 0.776$ : this corresponds to the first gap being maximum and to the vanishing of the second-order gap together with all gaps of even order.
  - 44 R. Magnusson and S.S. Wang, Appl. Phys. Lett. **61**, 1022 (1992).
  - 45 L. Li and J.J. Burke, Opt. Lett. **17**, 1195 (1992).
  - 46 E. Popov, Progr. Optics **31**, 141 (1993).
  - 47 M. Nevière, E. Popov and R. Reinisch, J. Opt. Soc. Am. A **12**, 513 (1995).
  - 48 D.D. Stancil, Appl. Opt. **35**, 4767 (1996).
  - 49 E.G. Loewen and E. Popov, *Diffraction Gratings and Applications* (Dekker, New York, 1997).
  - 50 T. Tamir and S. Zhang, J. Opt. Soc. Am. A **14**, 1607 (1997).
  - 51 D. Rosenblatt, A. Sharon, and A.A. Friesem, IEEE J. Quantum Electron. **33**, 2038 (1997).
  - 52 S.M. Norton, T. Erdogan, and G.M. Morris, J. Opt. Soc. Am. A **14**, 629 (1997).
  - 53 S.M. Norton, G.M. Morris, and T. Erdogan, J. Opt. Soc. Am. A **15**, 464 (1998).
  - 54 D.L. Brundrett, E.N. Glytsis, and T.K. Gaylord, Opt. Lett. **23**, 700 (1998).
  - 55 D.L. Brundrett, E.N. Glytsis, T.K. Gaylord, and J.M. Bendickson, J. Opt. Soc. Am. A **17**, 1221 (2000).
  - 56 M. Nevière, E. Popov, R. Reinisch, and G. Vitrant, *Electromagnetic Resonances in Nonlinear Optics* (Gordon and Breach, Amsterdam, 2000).
  - 57 P. Lalanne and E. Silberstein, Opt. Lett. **25**, 1092 (2000).
  - 58 S. Nilsen-Hofseth and V. Romero-Rochín, Phys. Rev. E **64**, 36614 (2001).
  - 59 Q. Cao, P. Lalanne, and J.-P. Hugonin, J. Opt. Soc. Am. A **19**, 335 (2002).
  - 60 The perturbative treatment of the coupling to radiative modes is analogous to that introduced by Ochiai and Sakoda<sup>23</sup>, however in the present method the dielectric modulation described by the tensor  $\epsilon_{\mathbf{G},\mathbf{G}'}$  is treated exactly, thereby going beyond the nearly-free-photon approximation of Ref. 23.
  - 61 C.K. Carniglia and L. Mandel, Phys. Rev. D **3**, 280 (1971).
  - 62 V.M. Agranovich, and V.E. Kravtsov, Solid State Commun. **55**, 85 (1985).
  - 63 It is known in the grating literature that the application of coupled-wave analysis to the case of TM polarization is more difficult and special methods are needed to stabilize numerical convergence, as discussed by Ph. Lalanne and G. M. Morris, J. Opt. Soc. Am. A **13**, 779 (1996).
  - 64 K.M. Ho, C.T. Chan, and C.M. Soukoulis, Phys. Rev. Lett. **65**, 3152 (1990).
  - 65 In Ref. 55 a Brillouin diagram for the losses is shown, i. e., the imaginary part of the wavevector is displayed as a function of frequency. The meaning of the loss diagram is therefore different from those in Fig. 7, in particular the imaginary part of the wavevector is largest in the photonic gap regions.